

NUMERICAL MODELLING OF A PITCHING AIRFOIL

K.A. Ahmad*, M.Z. Abdullah¹ and J.K. Watterson²

¹School of Aerospace Engineering, Engineering Campus
Universiti Sains Malaysia, Malaysia.

²School of Mechanical and Aerospace Engineering, Faculty of Engineering and
Physical Sciences, Queen's University of Belfast, United Kingdom.

ABSTRACT

The RANS code FluentTM 6.1 is used to predict the flow field around a pitching NACA 0012 airfoil. A hybrid mesh was employed in the computational domain and different mesh configurations are tested and the results are compared. Two-equation turbulence models namely $k-\epsilon$, $r k-\epsilon$, $k-\omega$, and SST $k-\omega$ were tested and their results are compared. The turbulence model that gives the best agreement with the experimental data for 2D case is SST $k-\omega$ with y^+ value set to 1. Mesh and time step dependency checks are also performed and the results show that the c_l and c_d are not effected by varying the time step and mesh parameters. However it was observed that time step and mesh independent predictions for the c_m hysteresis loop could not be obtained.

Keywords: *Airfoil modelling, NACA airfoil, flow field, turbulent model, hysteresis loop.*

1.0 INTRODUCTION

Dynamic stall is an unsteady phenomenon that only occurs when lifting surfaces such as an airfoil pitches unsteadily to angles exceeding the static stall angle, causing the aerodynamic lift to increase beyond the maximum value for unstalled conditions. The aerodynamic forces and moment overshoots are usually associated with the formation of the dynamic stall vortex (DSV) which first appears at the leading edge of the lifting surface (in this case it is an airfoil) and travels along the lifting surface until it separates at the trailing edge. However, after the DSV detaches from the airfoil and moves into the wake, the lift decreases abruptly. Some researchers relate these overshoots to the delay of the separation rather than the formation of the dynamic stall vortex [1].

The unsteady aerodynamic characteristics resulting from the rate of change in angle of attack and can be significantly different from those of the static case. Under oscillatory or transient motion, the vortices which are created by leading edge separation change strength and position as a function of time varying angle of attack. Therefore, the location of vortex breakdown will likewise become time

* Corresponding author: aekamarul@eng.usm.my

dependent. These changes in the vortex flow do not take place immediately with the dynamic motion, due to the convective time lag of adjusting flow field.

Over the past three decades, the dynamic stall phenomenon has been investigated through experimental and numerical approaches and a significant progress has been made to understand the general features of the dynamic stall. Examples of past theoretical and experimental works can be found in [2], [3], and [4]. More recent experimental works can be found in [5] and [6]. Examples of numerical works can be found in the papers of [1], [7], [8], [9], and [10]. These numerical studies have analysed the dynamic stall phenomenon in laminar and turbulent flow conditions.

The objective of this investigation is to perform numerical investigation on a pitching 2D NACA 0012 model. The RANS solver Fluent 6.1TM was used to predict this unsteady flow problem. Calculations were conducted with different two-equation turbulence models with different type of wall treatments. The main reason of two-equation turbulence model because it offer reasonably good prediction with less computation time compared to other turbulence models. It also offers flexibility of different wall treatments to be used together with the turbulence models. The predictions were then compared to the previous experimental results.

2.0 NUMERICAL METHODS

2.1 Governing Equations

The integral form of the transport equation for a general scalar, ϕ , on an arbitrary control volume, V , which implemented in Fluent 6.1TM is as shown below:-

$$\frac{d}{dt} \int_V \rho \Phi (\bar{u} - \bar{u}_g) d\bar{A} = \int_{\partial V} \Gamma \Delta \Phi \cdot d\bar{A} + \int_V S_\Phi dV \quad (1)$$

The first and second terms on the left side of Equation (1) are the time derivative term and the convective term. The time derivative term indicates that the solution is changing with time. Meanwhile the first and the second terms on the right of equation 1 are the diffusive term and the source term. The term ∂V is used to represent the boundary of the control volume V . The SIMPLE algorithm was used for pressure-velocity coupling and second order spatial discretisation was used for all of the equations. The time derivative in Equation 1 can be discretised using Equation 2.

$$\frac{d}{dt} \int_V \rho \Phi dV = \frac{(\rho \phi V)^{n+1} - (\rho \phi V)^n}{\Delta t} \quad (2)$$

The indices n and $n+1$ denote, respectively, the quantity at the current and next time level. Meanwhile the $(n+1)$ th time level volume V^{n+1} is computed from Equation 3.

$$V^{n+1} = V^n + \frac{dV}{dt} \delta t \quad (3)$$

The term $\frac{dV}{dt}$ denotes the volume time derivative of the control volume.

In order to satisfy the grid conservation law, the volume time derivative of the control volume is computed from Equation 4.

$$\frac{dV}{dt} = \int_{\partial V} \vec{u}_g \cdot d\vec{A} = \sum_j^{n_f} \vec{u}_{gj} \cdot \vec{A}_j \quad (4)$$

The term n_f is the number of faces on the control volume and \vec{A}_j is the face area vector. The dot product $\vec{u}_{gj} \cdot \vec{A}_j$ on each control volume face is identical to the volume swept by the control volume face j over unit time:

$$\vec{u}_g \cdot d\vec{A} = \frac{\partial V_j}{\Delta t} \quad (5)$$

2.2 Geometry, Mesh and Boundary Conditions

Figure 1 shows a schematic diagram of the 2D computational domain. The size of the computational domain was chosen in order to obtain a domain-independent solution. For the 2D case, a hybrid mesh was employed to ensure accuracy of the flow simulations near the wall surfaces. Quad cells were used around the airfoil while triangular cells were used in the core of the flow. A mesh separation method was used so that when the airfoil rotates, its neighbouring quad cells also move with it. Hence the portion of quad cells remains unchanged thus maintaining the highest possible accuracy for the flow prediction near the wall (see Figure 1).

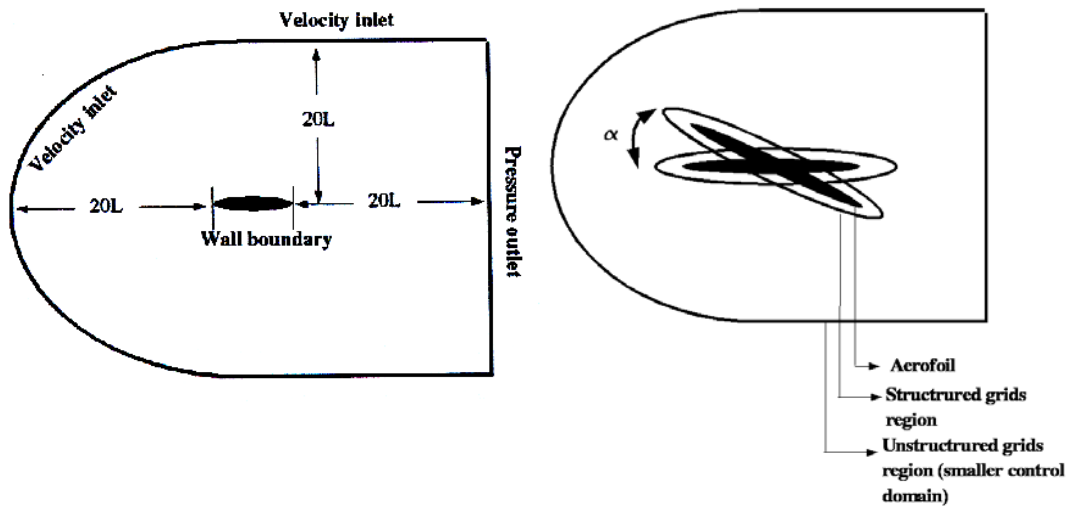


Figure 1: Computational domain and meshes of 2D pitching NACA 0012 airfoil

The prescribed pitching motion is based on the harmonic oscillation equations shown in the Equation 6.

$$\alpha = \alpha_{\min} + \frac{1}{2}(\alpha_{\max} - \alpha_{\min})(1 - \cos(\omega t)) \quad (6)$$

The unsteady motion of the pitching airfoil is characterized by the reduced frequency of the oscillation. This is defined by Equation 7. In the current study, the reduced frequency was chosen to be 0.15, the same as in the experiment.

$$F^t = \frac{\omega L}{2u_{\infty}} \quad (7)$$

A spring based smoothing method is used to govern the motion of the mesh. The edges between any two mesh nodes are idealized as a network of interconnected springs. The initial spacing of the edges before any boundary node will generate a force proportional to the displacement along all springs connected to the node. Using the Hook's law, the force on a mesh node can be written as

$$\vec{F}_i = \sum_j^{n_i} k_{ij}(\Delta\vec{x}_j - \Delta\vec{x}_i) \quad (8)$$

where $\Delta\vec{x}_j$ and $\Delta\vec{x}_i$ are the displacements of node i and its neighbor j , n_i is the number of neighboring nodes connected to node i , and k_{ij} is the spring constant (or stiffness) between node i and its neighbor j . The spring constant for the edge connecting nodes i and j is defined as

$$k_{ij} = \frac{1}{\sqrt{|\Delta\vec{x}_j - \Delta\vec{x}_i|}} \quad (9)$$

This method is appropriate for a triangular type of mesh since they can easily be idealized as springs.

2.3 Testing Condition and Analysis

Experiments performed by McCroskey et. al. were used for validation of 2D unsteady, fully turbulence flow solutions. The experimental results include hysteresis loops of lift, drag, and pitching moment. A time step of 1×10^{-3} sec was chosen and 60 sub-iterations per time step were performed. The Reynolds number, based on the freestream velocity was 1×10^6 . The airfoil cycle starts at $\alpha=50$ and the airfoil cycle amplitude is 20° . The solutions were computed with four main turbulence models, namely the k- ϵ , realizable k- ϵ , k- ω , and SST k- ω . Each turbulence model is tested with two or three different wall treatment approaches. If a wall function is used, then the wall y^+ value will be in the range of 30 to 60, whilst if a wall function is not in used, the wall y^+ approaches 1. Table 1 shows all the turbulence models that were used with their symbols.

Calculations were run for several cycles until periodicity was observed in the solutions. The average number of iterations for the solution to reach a steady state for each time step is about 120 iterations, and the simulations were performed using a serial version of FLUENT code. The time taken in most cases took about 72 hours on a Intel Pentium IV 2.66GHz. Solution periodicity was achieved after three cycles.

Table 1: Two equations turbulence models with specified symbols

Turbulent Model	Wall Treatment	No of cells	Symbol
k- ϵ	standard wall function	26670	ke I
	non-equilibrium wall function	26610	ke II
	two-layer near wall model	28370	ke III
reliable k- ϵ	standard wall function	26670	re I
	non-equilibrium wall function	26670	re II
	two-layer near wall model	28370	rke III
k- ω	standard wall function	26670	k ω I
	two-layer near wall model	28370	k ω III
SST k- ω	standard wall function	26670	SST k ω I
	two-layer near wall model	28370	SST k ω III

3.0 RESULTS

3.1 Validation of RANS Turbulence Models

Results for k- ϵ and rk- ϵ are shown in Figure 2. The lift coefficient values for k- ϵ I and II were predicted well for the early upstroke stage, but both models performed poorly when the airfoil approached 25° and during the downstroke cycle. The c_d and c_m plots (see Figures 2 (b) - (c)) show that both models delay the DSV separation (notice that the rapid increase in predicted values of c_d and c_m was delayed). It can be concluded that k- ϵ model does not have the capability to predict the nature of the dynamic stall. Meanwhile, the rk- ϵ I and II models managed to predict the essential features for the upstroke stage (see Figures 2 (d) - 2(f)). However the difference between the experimental results and the rk- ϵ I and II remains large for the high angle of attack. Nevertheless, both models managed to capture the formation and the detachment of the trailing edge vortex at the early stage of the downstroke. It is also clear that the rk- ϵ gives better agreement compared to standard k- ϵ . This superior performance is more pronounced in the c_l hysteresis loop. These trends were expected as rk- ϵ is designed to improve computations of separated flows. One also can see that having y^+ value equal to 1 did not help to improve the predictions.

Figure 3 shows the lift, drag, and pitching moment hysteresis loops for k- ω and SST k- ω turbulence models respectively. From the figures (see Figures 3(a) - 3(c)), it can be seen that the k- ω I and II managed to capture the trend of the

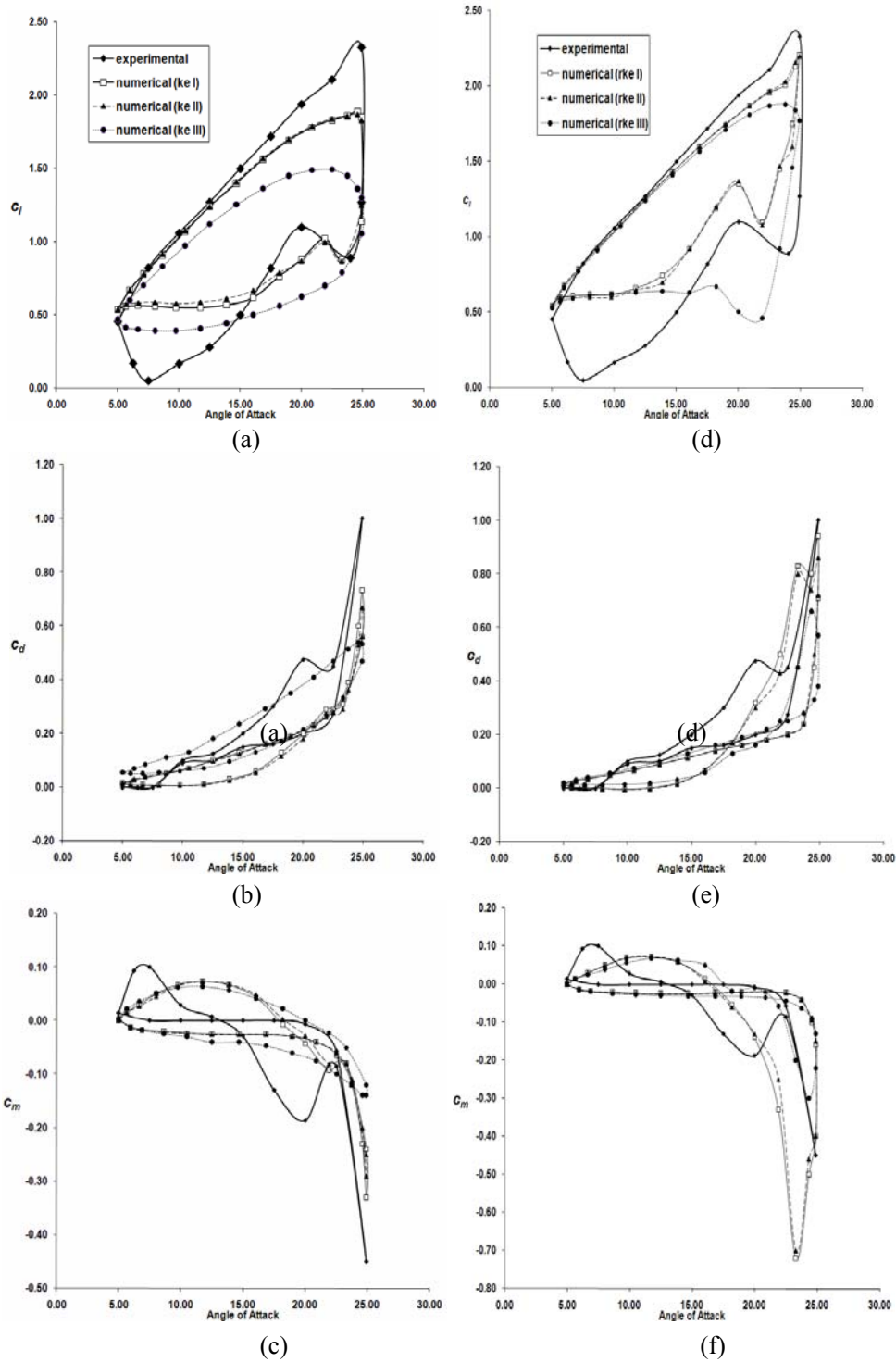


Figure 2: Hysteresis loops for k- ϵ ((a)-(c)) and rk- ϵ ((d)-(f))

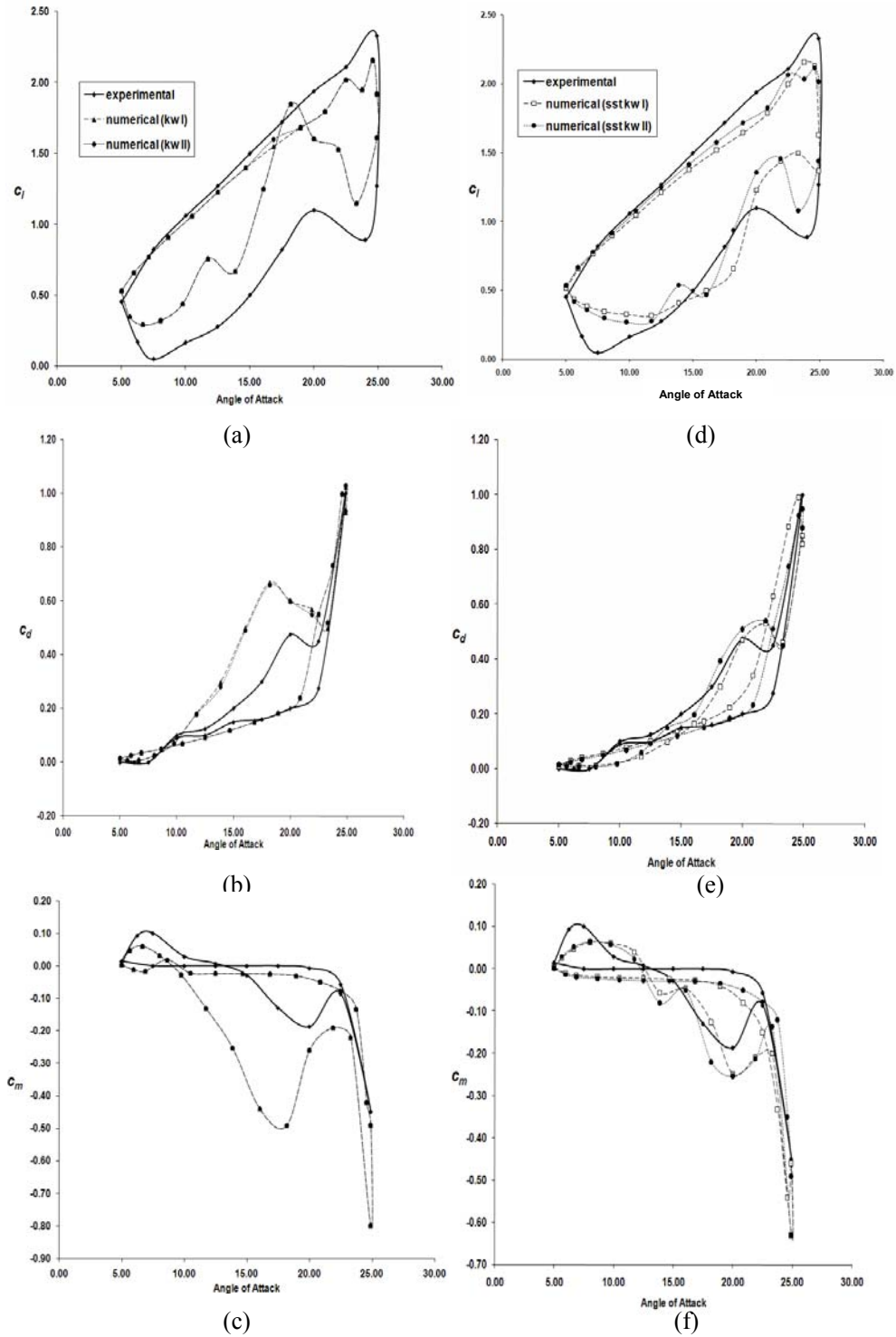


Figure 3: Hysteresis loops for $k-\omega$ ((a) - (c)) and SSTk- ω ((d) - (f))

hysteresis loops. Both models give reasonable agreement with the experimental data during the upstroke stage, but differed significantly for the downstroke stage. The lift overshoot during the downstroke stage probably was caused by the formation of a strong trailing edge vortex. This second vortex initially grows in size and then detaches from the airfoil surface and converts in the wake. The drag hysteresis loop shows that there was an early separation of DSV from the airfoil surface. Overall performances of both models are sufficient to predict the mean features of the dynamic stall phenomenon. Although the difference between computation and experimental data remains large, the general features of the flow are predicted reasonably well.

Meanwhile Figures 3(d) - 3(f) show that SST k- ω I and II predictions are in good agreement with the experimental results for the upstroke stage. In fact, the difference is smaller compared to the other turbulence models that have been tested. The SST k- ω I model predicts the lift overshoot nearly the same as the experiments. However, this model still fails to predict the formation of the trailing edge vortex. Meanwhile the SST k- ω II managed to predict the formation of the trailing edge vortex and its detachment. From the c_m hysteresis loop (see Figure 3 (f)), it can be seen that SST k- ω delays the separation of the dynamic stall vortex. This turbulence model will be used for all of the 2D computation in the remainder of this work. Overall performance is satisfactory especially for the SST k- ω II turbulence model.

3.2 Time Step and Mesh Dependency Analysis

Figures 4(a) - 4(c) show the hysteresis loops for SST k- ω with the time step of 1×10^{-3} sec (SST k- ω time step I) and 5×10^{-4} sec (SST k- ω time step II). One can see that varying the time step value, does not significantly affect the computational results. However, for the c_m value, the lower time step gives a more stabilized solution with fewer oscillations during the downstroke stage. Table 2 shows the symbols used for each model with different mesh size while Figures 4(d) - 4(f) show the hysteresis loops of various mesh sizes. The refinement of the mesh is focused on the suction surface of the airfoil as most of the crucial elements of the dynamic stall phenomenon occur on this surface. From these figures, it can be clearly seen that there is no significant change during the upstroke stage. The c_l loop shows that the increment of the mesh will reduce the gap between the computational and experimental results at the beginning of the downstroke stage. This increment also induces oscillations of c_l and c_m during the downstroke stage. It must be observed that the time step and mesh independent predictions of the c_m hysteresis loop have not been obtained. This implies that the predicted pressure distribution and evolution of the DSV are not time step or mesh independent.

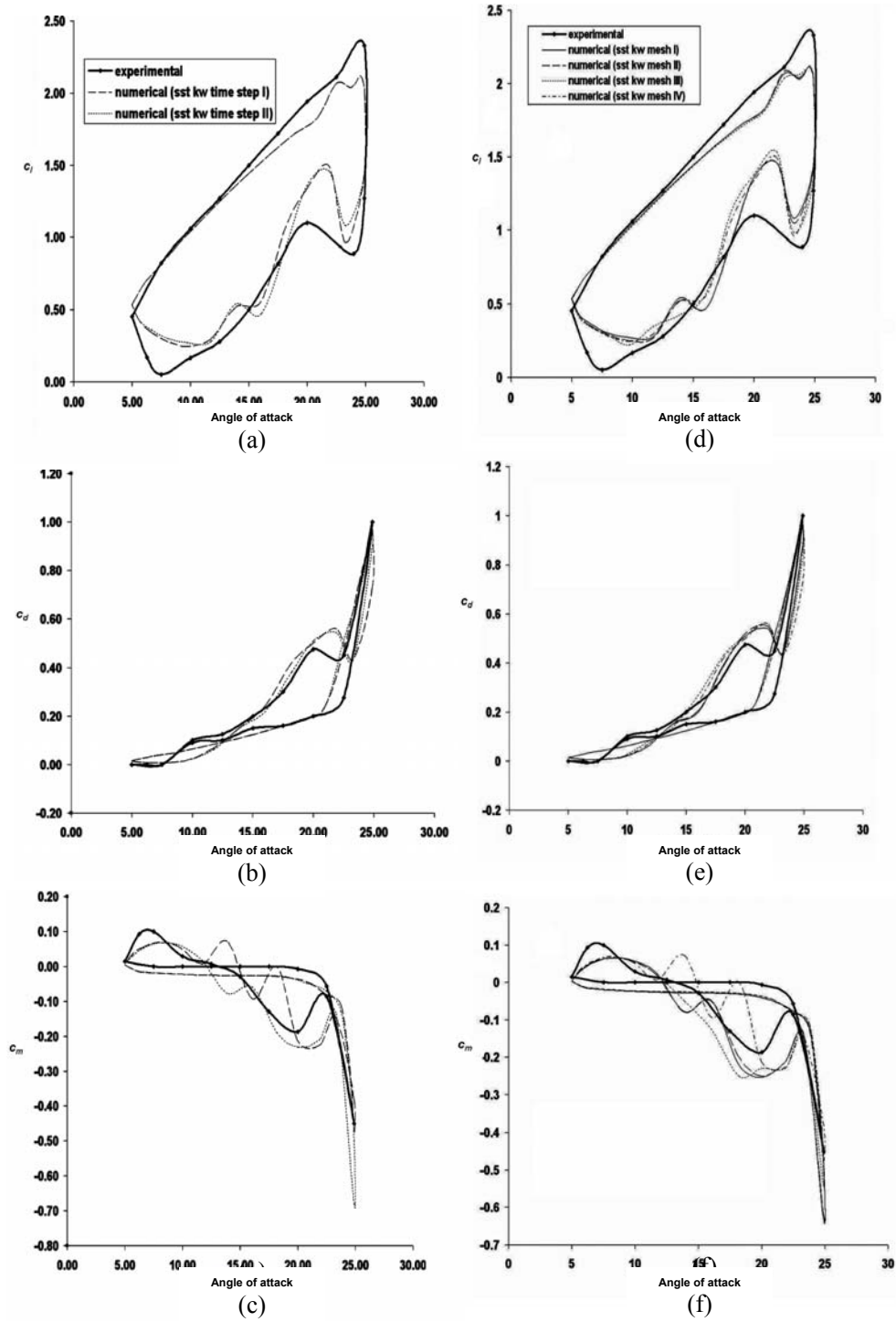


Figure 4: Parametric dependency study

Table 2: Various mesh sizes with specified symbols

Turbulent Model	Mesh Size	Symbol
SST k- ω	28370	sst k ω mesh I
	52573	sst k ω mesh II
	78627	sst k ω mesh III
	109025	sst k ω mesh IV

4.0 CONCLUSIONS

A RANS code has been used to predict the flow field around a pitching NACA 0012 airfoil. The results demonstrated that the best turbulence model that gives the best agreement with the experimental data is SST k- ω with y^+ value is set to 1. It was also found that the c_l and c_d were not effected by varying the time step and mesh parameters. However it was observed that time step and mesh independent predictions for the c_m hysteresis loop could not be obtained.

ACKNOWLEDGEMENTS

The authors would like to thank the Universiti Sains Malaysia for sponsoring the work (RU grant 814042).

NOMENCLATURE

- c_d Lift coefficient
- c_l Drag coefficient
- c_m Pitching moment coefficient
- k Turbulence kinetic energy
- F^+ Reduced frequency
- L Length of the object
- u_a Freestream velocity
- ω Natural frequency
- y^+ Local Reynolds number
- α Angle of vibration
- α_{\max} Maximum angle of pitch
- α_{\min} Minimum angle of pitch
- $d\alpha$ Range of the angle of pitch
- ϵ Dissipation rate of turbulence
- ω Specific turbulent dissipation rate

REFERENCES

1. Akbari, M.H., Price, S.J., 2003, Simulation of dynamic stall for a NACA 0012 airfoil using a vortex method, *Journal of Fluids and Structures*, 17, 855-874.
2. Theodorsen, T., 1979, General theory of aerodynamic instability and the mechanism of flutter, Report National Advisory Committee for Aeronautics, Report No 496, Dec.
3. McCroskey, W.J., 1977, Some current research in unsteady fluid dynamics-the 1976 freeman scholar lecture, *Journal of Fluids Engineering*, 8-39.
4. Ohmi, K., Coutanceau, M., Daube, O., Loc, T.P., 1991, Further experiments on vortex formation around and oscillating and translating airfoil at large incidences, *Journal of Fluid Mechanics*, 225, 607-630.
5. Panda, J., Zaman, K.B.M.Q., 1994, Experimental investigation of the flow field of an oscillating airfoil and estimation of lift from wake surveys, *Journal of Fluid Mechanics*, 265, 65-95.
6. Coton, F.N., Galbraith, R.A.M., JIang, D., and Gilmour., 1996, An experimental study of the effect of pitch rate on the dynamic stall of a finite wing, Royal Aeronautical Society, 17-18 July.
7. Carr, L.W., 1985, Progress in analysis and prediction of dynamic stall, AIAA, Atmospheric Flight Mechanics Conference, Snowmass, CO, August 19-21.
8. Tuncer, I.H., Wu, J.C., Wang, C.M., 1990, Theoretical and numerical studies of oscillating airfoils, *AIAA Journal*, 28, (9), Sept.
9. Ekaterinaris, J.A., Menter, F.R., 1994, Computation of oscillating airfoil flows with one and two equation turbulence models, *AIAA Journal*, 28, (12), Dec.
10. Barakos, G.N., Drikakis, D., 2000, Unsteady separated flows over manoeuvring lifting surfaces, *Phil. Trans. R. Soc. Lon.* 358, 3279-3291.